Journal of ELECTRONIC MATERIALS, Vol. 41, No. 11, 2012
DOI: 10.1007/s11664-012-2198-z

Crystal Structure and Morphology of Nanocrystalline TiN Thin Films

C.V. RAMANA,[1,2,4] S. WHITE,[1] N. ESPARZA,[1,2] V. RANGEL,[1,2] and A.L. CAMPBELL[3]

1.—Department of Mechanical Engineering, University of Texas at El Paso, El Paso, TX 79968, USA. 2.—Department of Materials Science and Engineering, University of Texas at El Paso, El Paso, TX 79968, USA. 3.—Materials and Manufacturing Directorate (RX), Wright-Patterson Air Force Base (WPAFB), Wright-Patterson Air Force Base, OH 45433, USA. 4.—e-mail: rvchintalapalle@utep.edu

Titanium nitride (TiN) thin films were grown employing radiofrequency (RF) magnetron sputtering under varying nitrogen gas flow rates. Characterization of the grown materials was done by grazing-incidence x-ray diffraction and scanning electron microscopy. The results indicate that the crystal structure and texture of the grown TiN layers are dependent on the ratio of nitrogen to argon in the reactive gas mixture during deposition. TiN coatings initially showed (111) preferred orientation, then mixed (111) and (002) texturing, followed by completely (002) texturing with increasing nitrogen content. The analyses indicate that the nitrogen incorporation into the layers and the associated chemistry determine the texturing and lattice parameters.

Key words: TiN films, reactive sputtering, crystal structure, texturing, lattice constant morphology

INTRODUCTION

Titanium (Ti) compounds, especially nitrides and oxides, find widespread use in various scientific and technological applications. The titanium nitride (TiN) system continues to be of great interest because of its unique physical, electrical, chemical, electrochemical, optical, and mechanical properties.[1–31] Due to their excellent physical and mechanical properties, TiN films have been used as wear- and corrosion-resistant coatings for industrial machinery tools[1–4] and as biocompatible wear-resistant coatings for implants and surgical components in biomedical engineering.[17,18] In addition to wear and corrosion, their lustrous color makes TiN coatings useful for decorative applications.[14–16] TiN films serve as metallization materials or diffusion barriers for metal interconnects in microelectronics.[19–21] The optical properties of TiN films make these materials interesting for application in solar cells.[15,22] Currently, there is strong interest in TiN nanostructured materials for electronics and energy-related technologies.[26–31] From an electronic material standpoint, significant attention has been directed towards understanding the electrical transport properties, electronic structure, optical properties, and charge-transfer ability of nanostructured TiN materials.[26–31]

TiN films can be produced using a wide variety of physical vapor deposition (PVD) methods. However, the microstructure of TiN films is very sensitive to the growth conditions.[1–22] Controlled growth, texturing, and composition of the TiN layers can significantly influence their properties, phenomena, and performance;[1–25] For instance, since the preferred crystallographic orientation has a strong influence on the resulting properties and performance, the texture development and associated mechanisms in thin TiN coatings have been the subject of numerous studies. It has been reported that the wear resistance of TiN coatings deposited on tools can be greatly increased for (111) orientation.[24,25] When used as a diffusion barrier coating, the (111) texturing of TiN is found to induce preferential growth of a (111) Al metal line that results in enhanced electromigration lifetime.[19] It has been demonstrated that the texturing of TiN

(Received November 13, 2011; accepted July 3, 2012; published online August 2, 2012)

films greatly influences interconnect thin-film stacks in integrated circuits.[32,33] Therefore, it is very important to understand the effect of process parameters, deposition temperature, and reactive pressure, which allows one to tune the microstructure and electronic properties of the TiN films at reduced dimensions and for a desired application. Specifically, the ratio of nitrogen to argon influences the electronic structure and electrical conductivity of the TiN films.[24,25,29] The present work was performed on thin TiN nanolayered, nanocrystalline films grown using reactive sputter deposition. Films were grown under varying nitrogen flow rates. The impetus is to understand the effect of nitrogen content on the growth, microstructure, and optical characteristics of the TiN nanocrystalline films. While the ultimate goal is to understand the effect of the flow rate of nitrogen gas and tune the conditions to obtain enhanced optical constants (e.g., index of refraction and extinction coefficient), the present work is focused on understanding the structure and morphology of TiN films. The results obtained on the growth behavior and surface morphology are presented and discussed herein.

EXPERIMENTAL PROCEDURES

TiN films were fabricated using radiofrequency (RF) magnetron sputter deposition while varying the reactive pressure. A 2-inch-diameter Ti metal target (99.99% purity; Plasmaterials Inc.) was used in reactive sputtering. The Ti target was placed on a 2-inch sputter gun at a distance of 8 cm from the substrate. Films were grown onto silicon (Si) (100) substrates. The silicon substrates were cleaned by standard Radio Corporation of America (RCA) cleaning. All the substrates were thoroughly cleaned and dried with nitrogen before introducing them into the deposition chamber. The deposition chamber was pumped down to base pressure of 6.6×10^{-5} Pa, and the sputtering pressure was kept at 0.33 Pa. High-purity argon (Ar, 99.999%) and nitrogen (N_2, 99.999%) were the working and reactive gas, respectively. The samples were grown with nitrogen flow rates that varied from 0 sccm to 50 sccm while keeping the pressure constant. The pressure and flow rate of Ar were monitored by closed-loop control using an MKS 627 BARATRON pressure transducer, MKS250 pressure controller, and MKS 247D four-channel readout. Before each deposition, the Ti target was presputtered for 10 min using only Ar and with the shutter above the gun closed. Sputtering power of 40 W was initially applied to the target while introducing Ar into the chamber to ignite the plasma. Once the plasma was ignited, the power was increased to 100 W and high-purity nitrogen (N_2) was released into the chamber for reactive deposition. The flow of Ar and N_2 and their ratio was controlled using MKS mass flow controllers. The deposition was carried out to obtain ~70-nm-thick TiN films.

To avoid interference by the substrate and obtain structural information of the TiN films, grazing-incidence x-ray diffraction (GIXRD) was performed. GIXRD measurements were performed using a Bruker D8 Advance x-ray diffractometer as a function of nitrogen gas flow rate. GIXRD patterns were recorded using Cu K_α radiation (λ = 1.54056 Å). The x-ray beam was fixed at grazing incidence of 0.5°. The scanning was performed in a 2θ range of 15° to 60° using the "detector scan" mode. The detector was independently moved to collect the diffraction pattern. From the x-ray diffraction data, the interplanar spacing (d_{hkl}) between atomic planes can be determined using Bragg's relation:

$$2d_{hkl} \sin\theta = n\lambda, \tag{1}$$

where λ is wavelength of the x-rays. TiN exhibits cubic structure in a wide range of compositions. Therefore, the lattice parameter (a) of the grown films can be determined using the relation

$$a = d_{hkl}\sqrt{h^2 + k^2 + l^2}, \tag{2}$$

where (hkl) are the Miller indices for the diffraction planes responsible for the observed XRD peaks. Surface imaging analysis was performed using scanning electron microscopy (SEM) via a high-performance, ultrahigh-resolution scanning electron microscope (Hitachi S-4800). Secondary electron imaging was performed on the TiN coatings grown on Si wafers. Grain detection, size analysis, and statistical analysis were performed using the software accompanying the SEM.

RESULTS AND DISCUSSION

The GIXRD patterns of TiN films are shown in Fig. 1 as a function of N_2 flow. It is evident that the N_2 flow strongly influences the crystal structure, degree of preferred orientation, and texturing. The observed peaks in XRD patterns are due to (111) and (002) reflections of TiN as indicated in Fig. 1. At low N_2 content, the grown TiN films exhibit a (111) preferred orientation. Films grown at 3 sccm to 6 sccm of N_2 exhibit a (111) texturing, while the texturing decreases with increasing N_2 flow. The (111) peak intensity and, hence, the preferred orientation continue to increase until N_2 flow of 10 sccm, at which point a decrease in (111) peak intensity coupled with the onset of (002) peak can be noticed. A further increase in N_2 flow rate to 15 sccm balances the (111) and (002) peak intensities; i.e., the (111) peak intensity decreases as the (002) peak intensity increases. It seems that the increased nitrogen flow causes a change in the microstructure of the TiN coating. A further increase in N_2 flow to 20 sccm or greater causes a complete change in the film pattern. It is evident that the (111) peak disappears totally at these higher N_2 flow values. An increase in the N_2 flow rate to 50 sccm resulted in an increase in the (002)

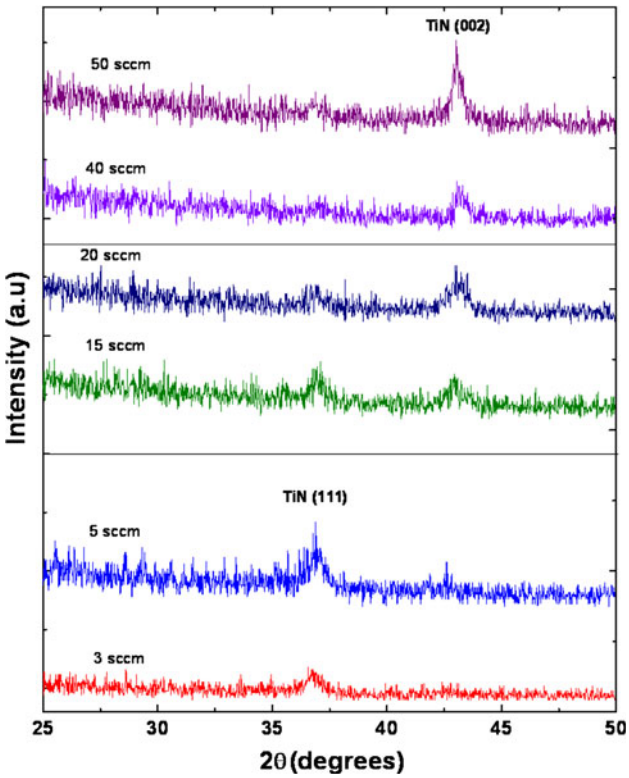

Fig. 1. XRD patterns of TiN films grown at various N_2 flow rates. The preferred (111) orientation of the films at lower N_2 flow rates is evident in the XRD patterns. The XRD patterns also indicate that the TiN films exhibit crossover to mixed (111) and (002) orientations for N_2 flow rates of ~15 sccm to 20 sccm and finally to a complete (002) preferred orientation at higher N_2 flow rates.

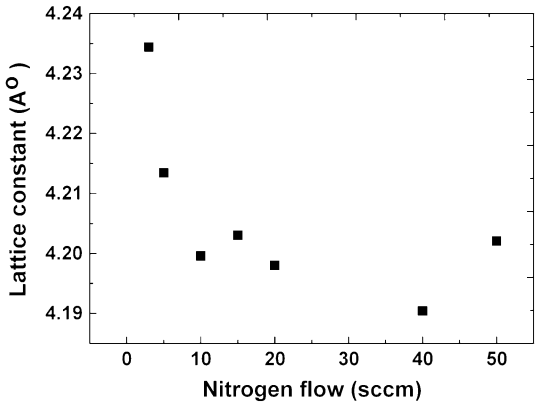

Fig. 2. Lattice parameter variation of TiN films with N_2 gas flow rate.

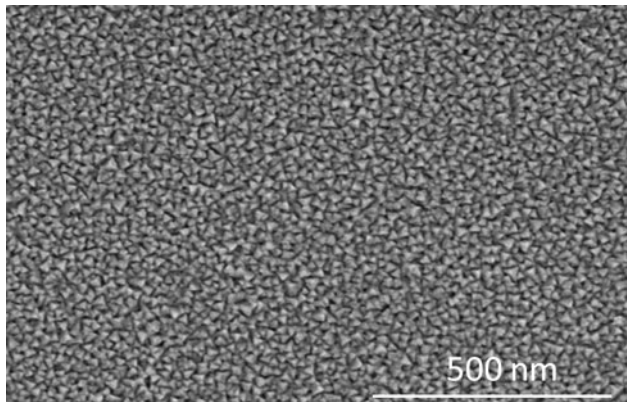

Fig. 3. SEM images of TiN films grown at N_2 flow of 3 sccm. The triangular morphology is evident in the image.

peak intensity. The TiN films initially textured in (111) preferred orientation were followed by a mixed (111) and (002) orientation and then finally the (002) preferred orientation. The origin of texturing in TiN films has been studied by many researchers in the past. The most commonly observed textures were (111), (002), or (220), or a mixture of these. The origin or driving force governing the specific texture, change in texture, and crossover of the preferred orientation has been the subject of numerous investigations.[3–8,13,34–39] Pelleg et al.[34] reported that the strain factor is important in determining the texturing of TiN films. Accordingly, the (111) orientation is preferred by thicker films, and the crossover from the (002) to the (111) orientation occurs for film thicknesses in excess of 0.5 μm. However, Greene et al. reported that the preferred orientation and associated transitions do not require the presence of stress and/or do not result from changes in stress state with increasing film thickness.[35,36] Patsalas et al.[37] also showed that there is no correlation between orientation and stress. Recently, based on computational work, Gall et al.[3] provided an atomistic explanation for the previously reported transition from the (111) to the (001) texture observed for sputter deposition of TiN in Ar/N_2 mixtures with increasing N_2 partial pressure P_{N2} and at constant P_{N2} with increasing N_2^+/Ti flux ratios incident at the growing film. They reported that growth of (111)-oriented grains is favored under conditions typical for reactive sputter deposition. However, the presence of excess atomic N (due, for example, to collisionally induced dissociation of energetic N_2^+ ions) leads to a reduced Ti diffusion length, an enhanced surface island nucleation rate, and a lower chemical potential on the (001) surface.[3] The combination of these effects results in preferential growth of (001) grains. Note that the TiN films in this work are grown at room temperature, where the adatom mobility is low. We, therefore, attribute the preferred (111) orientation of TiN films under low nitrogen flow rates to the kinetics. The anisotropy of adatom mobility drives the (111) texturing of the growing TiN film. However, under sufficient nitrogen flow rate, the adatom mobility increases due to ion–adatom momentum transfer that leads to the onset of (002) texturing associated with a decrease in (111) preferred orientation. The mixed (111) and (002) orientation with equal intensities is the crossover point, where the (002) preferred orientation dominates. Finally,

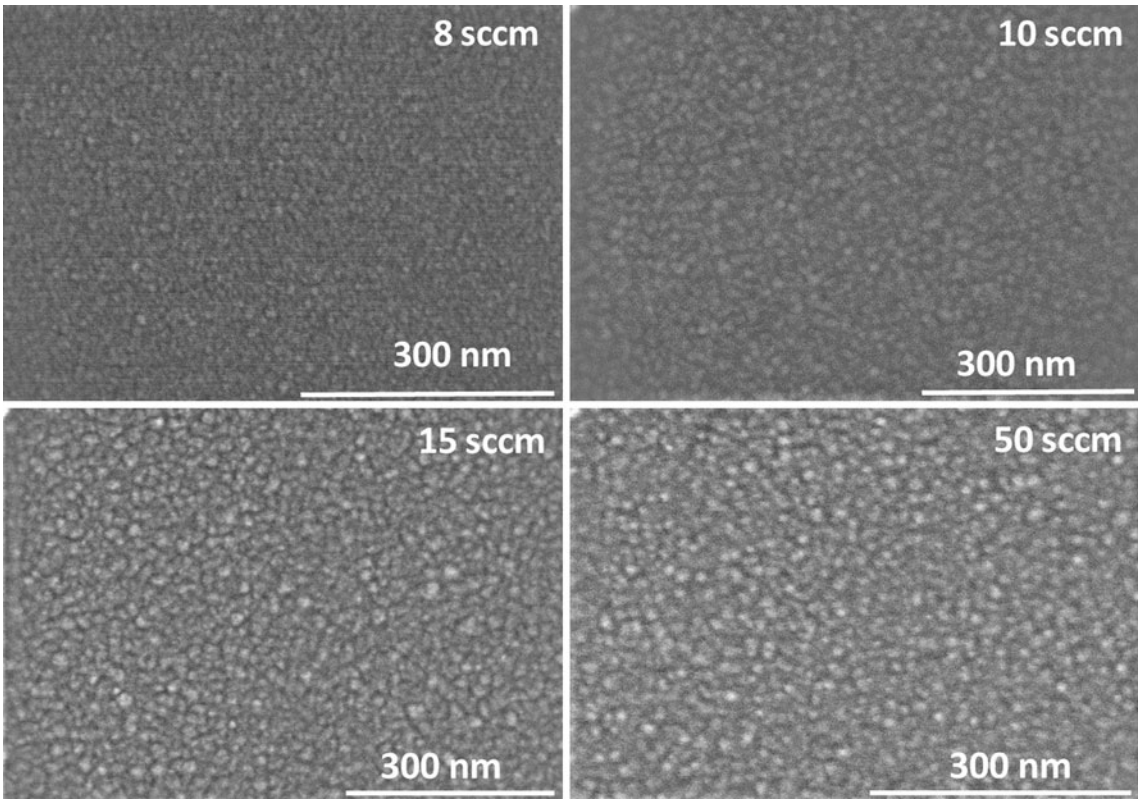

Fig. 4. SEM images of TiN films as a function of N_2 flow rates. A change in morphology with increasing N_2 flow is evident in these images.

under high nitrogen flow, the very high and significantly increasing nitrogen flux lead to the texturing of the films towards (002).

The lattice parameter values determined as a function of nitrogen gas flow rate indicate that the TiN films grown at lower nitrogen gas flow rates exhibit a lattice parameter of 4.234 Å, which is closer to that reported for bulk, stoichiometric TiN.[4–6] However, the lattice parameter decreases with increasing nitrogen gas flow rate. The variation of the lattice parameter of the TiN films is shown in Fig. 2. It is evident (Fig. 2) that the lattice parameter gradually decreases with increasing nitrogen gas flow rate in the reactive gas mixture during film deposition. The crystal formation, texturing, and lattice parameters are in turn controlled by the nitrogen stoichiometry in the grown TiN films. It has been reported that the lattice parameter of TiN_x decreases as the stoichiometry (i.e., N/Ti ratio) changes.[40–42]. Dekker et al.[41] have shown that vapor-synthesized TiN powders exhibit a linear functional dependence between the lattice parameter and the amount of nitrogen in the lattice. Comparing theoretical and experimental work, Gummez et al.[40] also suggested a linear correlation between lattice parameter and x values in TiN_x films. While the other factors are not accounted for at this time, the lattice parameter values for samples grown at lower nitrogen flow rates (<10 sccm) suggest that these TiN films may be near stoichiometric. A continuous decrease in the lattice parameter in this case can be attributed to the formation of non-stoichiometric TiN_x films given increasing nitrogen gas flow rate.

Within the cases presented, the surface morphology of TiN thin films via SEM measurements indicates that the effect of nitrogen content in the reactive gas mixture has a strong influence on the morphology evolution in Ti–N coatings. SEM images of Ti–N films grown at various nitrogen flow rates are shown in Figs. 3 and 4. Within these cases, the morphology changes and their dependence on nitrogen flow rate are evident. For low N_2 flow rates, the SEM images indicate that the surface morphology of TiN films is characterized by the presence of nanograins, which are strongly faceted. In addition, the characteristic feature of triangular-shaped morphology is clearly evident in the micrographs. A typical morphology behavior of the TiN films is shown in Fig. 3 for the representative case of films grown at 3 sccm N_2 flow rate. The grain morphology and grain boundary network can be noted from this image. The average size of these triangular-shaped grains is ~20 nm. These observed features agree well with the results reported by Banerjee et al.[5] for TiN films grown in Ar + N_2 reactive gas mixtures, as compared with He + N_2 reactive gas mixtures. However, in the present case, the observed mean value of the grain size is very low (20 nm) compared with reported

value (~50 nm) based on low-magnification transmission electron microscopy analysis.[5] The variance can be attributed to the slight difference in the experimental conditions and film thicknesses. Based on the presence of a strongly preferred (111) orientation in XRD and TEM measurements, it was suggested that the tetrahedral geometry is likely to be a manifestation of the four types of {111} planes in the face-centered cubic (fcc) unit cell. These places form a regular tetrahedron and contribute to such morphology. The observed (111) preferred orientation revealed by the XRD measurements of the work presented herein coupled with the TEM analysis presented in Ref. 5 promotes our belief that the specific morphology is induced by a similar mechanism and tetrahedral geometry.

With increasing N_2 flow rate, a change in morphology of the Ti–N coatings can be noted in correlation with the structural changes observed in the XRD analysis as shown in Fig. 4. While the morphology shown in Fig. 3 is maintained up to a N_2 flow rate of 10 sccm, the faceted morphology slowly turned into spherical grain morphology at flow rates beyond 10 sccm; for example, with N_2 flow rates between 15 sccm and 20 sccm, a mixture of faceted and spherical grain morphology is noted in SEM micrographs, and at these flow rates films exhibit the mixed (111) and (002) orientations. We, therefore, infer that the grains following the tetrahedral geometry are the ones responsible for the (111) orientations and the other grains, which are mostly spherical in shape, are responsible for (002) orientations. Increased N_2 content increases the energy and thereby the adatom mobility on the surface that initiates the growth towards the low-surface-energy (002).[3] However, at these flow rates, the adatom mobility is not sufficient to induced complete (002) preferred orientation, although the intensity of (002) peak is dominant compared with that of (111) at 20 sccm N_2 flow. Our results closely match the work of Mahieu et al.,[38,39] where it was reported that a N_2 flow rate of 14 sccm to 17 sccm induces a transition from (111) to (002) orientation. At N_2 flow of 25 sccm and above, the morphology is fully changed to dense spherical grains. The corresponding XRD patterns indicated that the TiN films exhibit a complete (002) preferred orientation.

CONCLUSIONS

TiN films were grown using RF magnetron sputtering for various nitrogen flow rates. The structure, surface morphology, and texture of these films were the focus of the investigation. The N_2 content in the reactive gas mixture has a significant effect on the texture, morphology, and lattice parameter of the Ti-N films. (111) preferred orientation is dominant for TiN films grown under low N_2 content. Ti-N films grown at N_2 rates between 15 sccm and 20 sccm exhibit mixed (111) and (002) texturing. At higher N_2 flow, the TiN films exhibit only the (002) preferred orientation. A direct correlation has been noted in the surface morphology evolution as a function of N_2 content. TiN films grown at low N_2 flow rates indicate the presence of strongly faceted nanograins in a triangular-shaped morphology, which changes to a mixture of triangular and spherical grain morphology in the N_2 range of 15 sccm to 20 sccm, where there is a mixed (111) and (002) orientation. The triangular-shaped morphology completely changes to nearly spherical grain morphology for higher N_2 flow rates, where the films exhibit only the (002) preferred orientation. The TiN films with (111) preferred orientation grown under low N_2 content (<10 sccm) exhibit lattice parameter values closer to that of stoichiometric TiN bulk and are believed to be nearly stoichiometric. Those TiN films grown at higher nitrogen gas flow rates are substoichiometric TiN_x films, which exhibit a continuous decrease in lattice parameter.

ACKNOWLEDGEMENTS

The authors at the University of Texas at El Paso (UTEP) acknowledge with pleasure the support of the Air Force Research Laboratory (Contract No. FA8650-05-D-1912) to perform this research work. The authors thank Nathanael Robinson, Associate Director of the Center for Space Exploration at UTEP, for critically reading the manuscript and insightful comments.

REFERENCES

1. H. Ljungcrantz, M. Oden, L. Hultman, J.E. Greene, and J.E. Sundgren, *J. Appl. Phys.* 80, 6725 (1996).
2. W.F. Wu, K.C. Tsai, C.G. Chao, J.C. Chen, and K.L. Ou, *J. Electron. Mater.* 446, 184 (2004).
3. D. Gall, S. Kodambaka, M.A. Wall, I. Petrov, and J.E. Greene, *J. Appl. Phys.* 93, 9086 (2003).
4. G. Abadias, *Surf. Coat. Technol.* 202, 2223 (2008).
5. R. Banerjee, R. Chandra, and P. Ayyub, *Thin Solid Films* 405, 64 (2002).
6. C. Ziebert and S. Ulrich, *J. Vac. Sci. Technol. A* 24, 554 (2006).
7. I. Petrov, P.B. Barna, L. Hultman, and J.E. Greene, *J. Vac. Sci. Technol. A* 21, S117 (2003).
8. W.J. Meng and T.J. Curtis, *J. Electron. Mater.* 515, 1229 (2006).
9. G. Abadias, Y.Y. Tse, Ph. Guerin, and V. Pelosin, *J. Appl. Phys.* 99, 113519 (2006).
10. H. Wang, A. Gupta, A. Tiwari, X. Zhang, and J. Narayan, *J. Electron. Mater.* 32, 994 (2003).
11. M. Marlo and V. Milman, *Phys. Rev. B* 62, 2899 (2000).
12. T.Q. Li, S. Noda, H. Komiyama, T. Yamamoto, and Y. Ikuhara, *J. Vac. Sci. Technol. A* 21, 1717 (2003).
13. Y.H. Cheng and B.K. Tay, *J. Cryst. Growth* 252, 257 (2003).
14. S. Kadlec, J. Musil, and J. Vyskcil, *Surf. Coat. Technol.* 54/55, 249 (1992).
15. N. Kalfagiannis and S. Logothetidis, *Rev. Adv. Mater. Sci.* 15, 167 (2001).
16. S. Niyomsoan, W. Grant, D.L. Olson, and B. Mishra, *Thin Solid Films* 415, 187 (2002).
17. S. Piscanec, L.C. Ciacchi, E. Vesselli, G. Comelli, O. Sbaizero, S. Meriani, and A. De Vita, *Acta Mater.* 52, 1237 (2004).
18. M.T. Raimondi and R. Pietrabissa, *Biomaterials* 21, 907 (2000).

19. J.S. Chun, I. Petrov, and J.E. Greene, *J. Appl. Phys.* 86, 3633 (1999).
20. L. Gao, J. Gstöttner, R. Emling, M. Balden, Ch. Linsmeier, A. Wiltner, W. Hansch, and D. Schmitt-Landsiedel, *Microelectron. Eng.* 76, 76 (2004).
21. M. Moriyama, T. Kawazoe, M. Tanaka, and M. Murakami, *Thin Solid Films* 416, 136 (2002).
22. G.M. Matnenoglou, S. Logothetidis, and S. Kassavetis, *Thin Solid Films* 511–512, 453 (2006).
23. Y. Pihosh, M. Goto, A. Kasahara, T. Oishi, and M. Tosa, *Appl. Surf. Sci.* 244, 244 (2005).
24. J.-E. Sundgren, *Thin Solid Films* 128, 21 (1985).
25. M. Kobayashi and Y. Doi, *Thin Solid Films* 111, 259 (1984).
26. S. Dong, X. Chen, L. Gu, X. Zhou, H. Xu, H. Wang, Z. Liu, P. Han, J. Yao, L. Wang, G. Cui, and L. Chen, *ACS Appl. Mater. Interfaces* 3, 93 (2011).
27. X. Lin, G. Zhao, L. Wu, G. Duan, and G. Han, *J. Alloys Compd.* 502, 195 (2010).
28. M.M. Ottakam Thotiyl, T. Ravi Kumar, and S. Sampath, *J. Phys. Chem. C* 114, 17934 (2010).
29. K. Vasu, M. Ghanashyam Krishna, and K.A. Padmanabhan, *Thin Solid Films* 519, 7702 (2011).
30. H. Xu, X. Zhang, C. Zhang, Z. Liu, X. Zhou, S. Pang, X. Chen, S. Dong, Z. Zhang, L. Zhang, P. Han, X. Wang, and G. Cui, *ACS Appl. Mater. Interfaces* 4, 1087 (2012).
31. L.P.B. Lima, J.A. Diniz, I. Doi, and J. Godoy Fo, *Microelectron. Eng.* 92, 86 (2012).
32. D.P. Tracy, D.B. Knorr, and K.P. Rodbell, *J. Appl. Phys.* 76, 2671 (1994).
33. K. Abe, Y. Harada, and H. Onoda, *Appl. Phys. Lett.* 71, 2782 (1997).
34. J. Pelleg, L.Z. Zevin, and S. Lungo, *Thin Solid Films* 197, 117 (1991).
35. J.E. Greene, J.-E. Sundgren, L. Hultman, I. Petrov, and D.B. Bergstrom, *Appl. Phys. Lett.* 67, 2928 (1995).
36. L. Hultman, J.-E. Sundgren, J.E. Greene, D.B. Bergstrom, and I. Petrov, *J. Appl. Phys.* 78, 5395 (1995).
37. P. Patsalas, C. Charitidis, and S. Logothetidis, *Surf. Coat. Technol.* 125, 335 (2000).
38. S. Mahieu, P. Ghekiere, G. De Winter, R. De Gryse, D. Depla, G. Van Tendeloo, and O.I. Lebedev, *Surf. Coat. Technol.* 200, 2764 (2006).
39. S. Mahieu, P. Ghekiere, G. De Winter, S. Heirwegh, D. Depla, R. De Gryse, O.I. Lebedev, and G. Van Tendeloo, *J. Cryst. Growth* 279, 100 (2005).
40. M. Guemmaz, A. Mosser, R. Ahuja, and J.C. Parlebas, *Int. J. Inorg. Mater.* 3, 1319 (2001).
41. J.P. Dekker, P.J. van der Put, H.J. Veringa, and J. Schoonman, *J. Mater. Chem.* 4, 689 (1994).
42. S. Nagakura and T. Kusunoki, *J. Appl. Crystallogr.* 10, 52 (1977).